Materials Research. 2024; 27:e20240036
DOI: https://doi.org/10.1590/1980-5373-MR-2024-0036

Electromagnetic Interference Shielding Effectiveness of Clay, Alumina, and Carbon Nanotubes Based on Epoxy Nanocomposites

***Felipe Carlos dos Reis*[a*], *Carlos Vinicios Opelt*[b], *Luiz Antonio Ferreira Coelho*[c], *Maurício Ribeiro Baldan*[d], *Bruno Ribeiro*[e], *Mirabel Cerqueira Rezende*[a]**

[a]*Universidade Federal de São Paulo (UNIFESP), Instituto de Ciência e Tecnologia, São José dos Campos, SP, Brasil.*
[b]*Universidade do Estado de Santa Catarina (UDESC), Departamento de Tecnologia Industrial, São Bento do Sul, SC, Brasil.*
[c]*Universidade do Estado de Santa Catarina (UDESC), Centro de Ciências Tecnológicas, Joinville, SC, Brasil.*
[d]*Instituto Nacional de Pesquisas Espaciais (INPE), São José dos Campos, SP, Brasil.*
[e]*Instituto de Pesquisas Tecnológicas (IPT), São José dos Campos, SP, Brasil.*

Received: January 26, 2024; Revised: May 17, 2024; Accepted: June 21, 2024

In this work, epoxy resin-based composites reinforced with nanoclays, nanoalumina, carbon nanotubes (CNTs) (0.15, 0.50, and 1.50% vol were submitted to morphological characterization by scanning (SEM) and transmission (TEM) electron microscopies, electrical tests through electrical impedance spectroscopy, and electromagnetic analyses (scattering parameters), in the frequency range of 8.2 to 12.4 GHz. SEM images of the CNT composite revealed nanotube clusters in the matrix. The proximity between the CNTs is corroborated by the increase in the electrical conductivity of the composite due to the formation of a long-range electron transport network, which favored the polarization effect, absorption losses (SE_A = 1.33 dB), reflection (SE_R = 3.38 dB) and reflection loss (RL = -6.61 dB at 10.8 GHz). Composites with nanoclays and nanoalumina showed no significant electrical and electromagnetic results.

Keywords: *EMI shielding, CNTs, epoxy composites, nanoalumina, nanoclays, microwave absorption.*

1. Introduction

Electromagnetic compatibility (EMC) is the ability to operate without introducing electromagnetic disturbances into the environment, in other words, it would be the absence of electromagnetic interference (EMI)[1]. Electromagnetic incompatibility causes malfunction of communication systems and transmission signals and can even cause information leakage. Therefore, electromagnetic shields are highly recommended for sensitive electronic equipment against electromagnetic radiation[2]. The function of the shielding material is to establish the boundaries of radiated energy, eliminating or reducing the effects of electromagnetic interference inside.

The blockage of electromagnetic wave transmission can occur by reflection, absorption, or multiple reflections inside the material[3]. The reflection mechanism is due to charge carriers interacting with the electromagnetic wave, being the primary shielding mechanism. The energy transmitted on the surface can still be dissipated as heat inside the material through dielectric and/or magnetic losses, which defines an absorbing material. The phenomenon of multiple reflections is usually disregarded in shielding efficiency calculation, trending to be more significant in heterogeneous materials with interfaces and/or pores, in which the electromagnetic wave is trapped, intensifying the losses[4].

Absorption is the most efficient mechanism for attenuating electromagnetic waves by reducing unwanted emissions (secondary pollution)[5]. Another advantage is the possibility of using semiconductor materials such as composites and conductive polymers. Reflecting materials, however, are restricted almost exclusively to metals, in which reflection is due to high electrical conductivity[6]. On the other hand, satisfactory absorption results are achieved with moderate conductivity, which makes the manufacturing of absorbing materials extremely attractive.

The development of absorbers in the microwave region (0.3-300 GHz), is of great importance, highlighting the X-band (8.2-12.4 GHz), due to the wide use of this frequency range in operations and communication of modern electronic devices used in defense systems and civil applications, such as cellphones signal relays, television, and climate monitoring sensors[7]. Microwaves can also be used in radars, which makes the processing of absorbing material heavily requested for stealth technology in defense systems and military platforms[8]. The variety of possible applications turns into necessary absorbers that show flexibility and lightweight. In this scenario, polymer composites are attractive for

*e-mail: fecreis@hotmail.com

their multifunctionality and tailoring properties by adding reinforcements. This combination may result in low-cost materials, easy processability, and good mechanical, thermal, and electrical properties[9].

Conducting reinforcements can increase shielding efficiency by improving the dielectric and magnetic properties of an insulating polymer matrix by creating interfaces and dipoles, forming a long-range electron transport network with a critical reinforcement concentration. The percolation threshold is achieved using conductive nanoparticles, whose high aspect ratio increases the probability of particle-particle contact and electrical interaction[10]. Thus, nanometric reinforcements incorporated in polymers are a viable strategy to maximize the shielding effectiveness of composites with low load filler content.

The maximum conversion of microwave energy into heat is achieved by a match between air and shielding material impedances, minimizing reflection losses[11]. In this sense, the electromagnetic wave can penetrate within the material, resulting in polarization or conduction losses by the Joule effect. Polarization is more relevant over 1 MHz, so microwave absorption is mostly given by electrical losses between conductive chargers when the composite exceeds the percolation threshold[12].

CNTs are allotropic forms of carbon in which covalently bonded atoms are organized in a honeycomb structure (2D). CNTs are observed when this structure forms cylindrical tubes with diameters on the nanometric scale and excellent electronic and charge transfer properties, given to the free electrons of the orbital p[13,14]. In this perspective, the development CNT based composites have been showing promising results of electromagnetic attenuation, given the high electrical conductivity of this carbon material[15-24].

In the literature, alumina and montmorillonite (MMT) nanoparticles are also used to refine the dielectric properties of materials and improve the multifunctional performance of composites. MMT particles are promising fillers due to their large surface area, high aspect ratio, and layered structure, which may enhance the shielding properties of the polymer matrix and its thermal stability[25,26]. Nanoalumina is a low-cost particle known for its excellent mechanical properties (Young modulus ~ 375 GPa), high thermal stability, excellent electrical insulation properties, and significant surface area[27].

In this regard, studies can be carried out in the area of electromagnetic shielding materials to analyze the effect of each particle on the electrical properties of composites, which motivates this work to elucidate the shielding mechanism through the electromagnetic, electrical, and morphological characterization of epoxy resin reinforced with nanoclays, nanoalumina, and carbon nanotubes.

2. Experimental

2.1. Materials

The samples were prepared using a procedure described in previous works[28-30], where specimens of type CT (Compact Tension) of dimensions 28 mm x 14 mm x 3 mm were obtained for fracture mechanic studies. The reinforcement used for the manufacture of nanocomposites were multi-walled carbon nanotubes - CNT (C 150P, Bayer, Baytubes, mean external diameter of 13 nm and length larger than 1 μm), nanoalumina (γ-Al_20_3, Nanum, mean diameter of 20-60 nm), sodium montmorillonite clay - MMT-Na+ (Cloisite Na+, Southern Clay, particle dimension of 25 μm), and organophilic montmorillonite clay - MMT-30B (Cloisite 30B, Southern Clay, particle dimension of 10 μm). Here it is important to highlight that the montmorillonite platelets are usually intercalated by sodium ions (as in Cloisite Na+). The substitution of these ions by ammonium salts (as in Cloisite 30B) is made to promote an organophilic behavior but ends up leading to an increase in the distance between platelets. From 1.17 nm in Cloisite Na+ to 1.85 nm in Cloisite 30B. Table 1 displays all the studied samples.

The matrix used in the prepared formulations was a bicomponent novolac epoxy-phenol resin (Araldite LY 5052 and Hardener Aradur HY 5052, Huntsman). The modifications were made by adding different nanoparticles in different volume fractions (0.15%, 0.5%, and 1.5% vol). In short, the preparation was carried out by high-energy sonication (Sonics VCX 750 to 180 W) and magnetic agitation of the nanoparticles in epoxy resin with a hardener until the energy added by the sonication process reached 400 J/g. The mixture was degassed to favor the removal of air and volatiles. The curing process was performed in silicone molds at room temperature for 24 h, with post-cure at 100 °C for 4 h. A more detailed description of the manufacturing procedure, as well as the overall mechanical behavior, may be found in previous publications[28-30].

2.2. Methods

The preparation of the specimens was performed by cutting half the length of the fractured piece using a micro grinding Dremel 3000 to obtain small specimens with 22.86 mm long, 10.16 mm wide, and 3 mm thick for the electromagnetic analyses (Figure 1).

2.3. Characterization

2.3.1. Field emission gun scanning electron microscopy (FEG-SEM)

The morphology of the samples was performed by FEG-SEM. As identified in Figure 1b, they were initially

Table 1. Samples prepared with different volume concentrations of nanofillers.

Sample code	Type of filler	Polymer matrix	vol. [%]
E	-	Epoxy Resin Araldite LY 5052	-
Al_0.15	Al_2O_3	Epoxy Resin Araldite LY 5052	0.15
Al_0.50			0.50
Al_1.50			1.50
CNT_0.15	MWCNTs	Epoxy Resin Araldite LY 5052	0.15
CNT _0.50			0.50
CNT _1.50			1.50
MMT B _0.15	MMT-30B	Epoxy Resin Araldite LY 5052	0.15
MMT B _0.50			0.50
MMT B _1.50			1.50
MMT A _0.15	$MMT\text{-}Na^+$	Epoxy Resin Araldite LY 5052	0.15
MMT A _0.50			0.50
MMT A _1.50			1.50

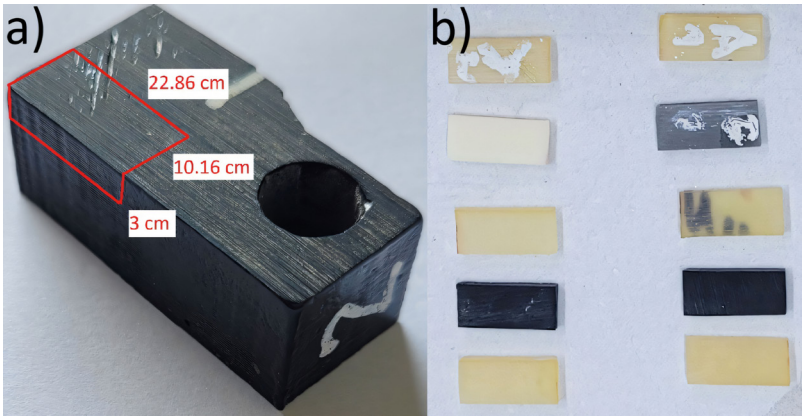

Figure 1. (a) Cutting scheme performed on CT samples and (b) example of specimens obtained after sanding.

fractured using pliers, subsequently sectioned and positioned in aluminum stubs with conductive carbon tape for the metallization process (gold/palladium alloy (Au-Pd): Q150R ES, quantum brand). The images were obtained using a high-resolution FEG scanning electron microscope (SEM TESCAN-MIRA3) at an accelerating voltage of 5 kV.

2.3.2. Transmission electron microscopy (TEM)

To corroborate the FEG-SEM analyses, TEM was used to evaluate the distribution/dispersion of nanoparticles in the nanocomposites, using samples with about 50 nm thickness. For this, ultrathin sections of the different nanocomposites were obtained using a RCM Power Tome X Ultramicrotome, with a diamond knife at room temperature, and analyzed in a JEOL JEM-2100 microscope.

2.3.3. Electrical impedance spectroscopy

The AC conductivity and relative permittivity were obtained from measurements by electrical impedance spectroscopy (Solartron SI 1260 Impedance/Gain-phase Analyzer) and applying 0.5 V voltage in the frequency range of 1 to 10^6 Hz. These analyses were conducted from the formation of electrodes through the metallization of the specimens with a thin layer of a gold/palladium alloy on the two surfaces perpendicular to the direction in which the impedance is performed.

2.3.4. Electromagnetic characterization

The electromagnetic behavior of the specimens (22.86 mm X 10.16 mm X 3.0 mm) was characterized in the frequency range of 8.2 to 12.4 GHz (X band) with the measurement of the scattering parameters (S-parameters), electrical permittivity, and magnetic permeability. The complex scattering parameters (S_{11} and S_{21}) express the total shielding effectiveness (SE_T) and its three main components: the reflection of the wave (SE_R), the internal absorption (SE_A), and secondary multiple-reflections (SE_M) inside the material by using Equations 1-3[31]. In the present work, the SE_M was neglected.

$$SE_T = SE_R + SE_A + SE_M \quad (1)$$

$$SE_R = -10\log_{10}(1-R) \quad (2)$$

$$SE_A = -10\log_{10}\left(\frac{T}{1-R}\right) \quad (3)$$

The tests were carried out using a vector network analyzer (VNA) (Agilent Technologies, model PNA-L N5235A, and serial number MY55451236) coupled to a rectangular waveguide (WR-90 model). Regarding reflection loss measurements, these were obtained with the same set of equipment, differing only by using an aluminum metal plate on the back of the sample holder.

3. Results and Discussions

3.1. FEG-SEM and TEM

All fracture surfaces shown in Figure 2 exhibit an irregular aspect, with numerous secondary cracks, resulting in different propagation planes. This is a direct result of the use of pliers to fracture the specimens since it promotes a mixed-mode loading condition (pressure + bending). Nonetheless, these irregular surfaces enlighten some characteristics of the nanoparticle dispersion/distribution. To further explore these morphological aspects, Figure 3 shows TEM images obtained for the same nanocomposites.

Figure 2a shows some regions with small wormlike aspects (highlighted by dotted white circles), which are very similar to the aspects shown by Opelt et al.[29]. In this work of literature, the occurrence of the crack bridging - pull-out mechanism in nanocomposites with a fraction of 0.5% vol. of CNTs was identified by using a higher magnification of the regions containing these wormlike aspects. Therefore, it is possible to assume that the occurrence of a similar aspect suggests the occurrence of the same toughening mechanism, i.e., crack bridging – pull-out mechanism. However, it is important not to confuse these wormlike aspects with the ribbons fractographic aspect (identified by white arrows), which occurs due to the overlap of cracks propagating in slightly different planes[32]. In addition, Figure 3a shows that the CNTs remained as a small agglomerate, with some loose CNTs in the neighborhood of this agglomerate.

Regarding the alumina nanocomposites, Figure 2b exhibits regions with a particulate texture on the fracture surface (marked by white circles), which implies the presence

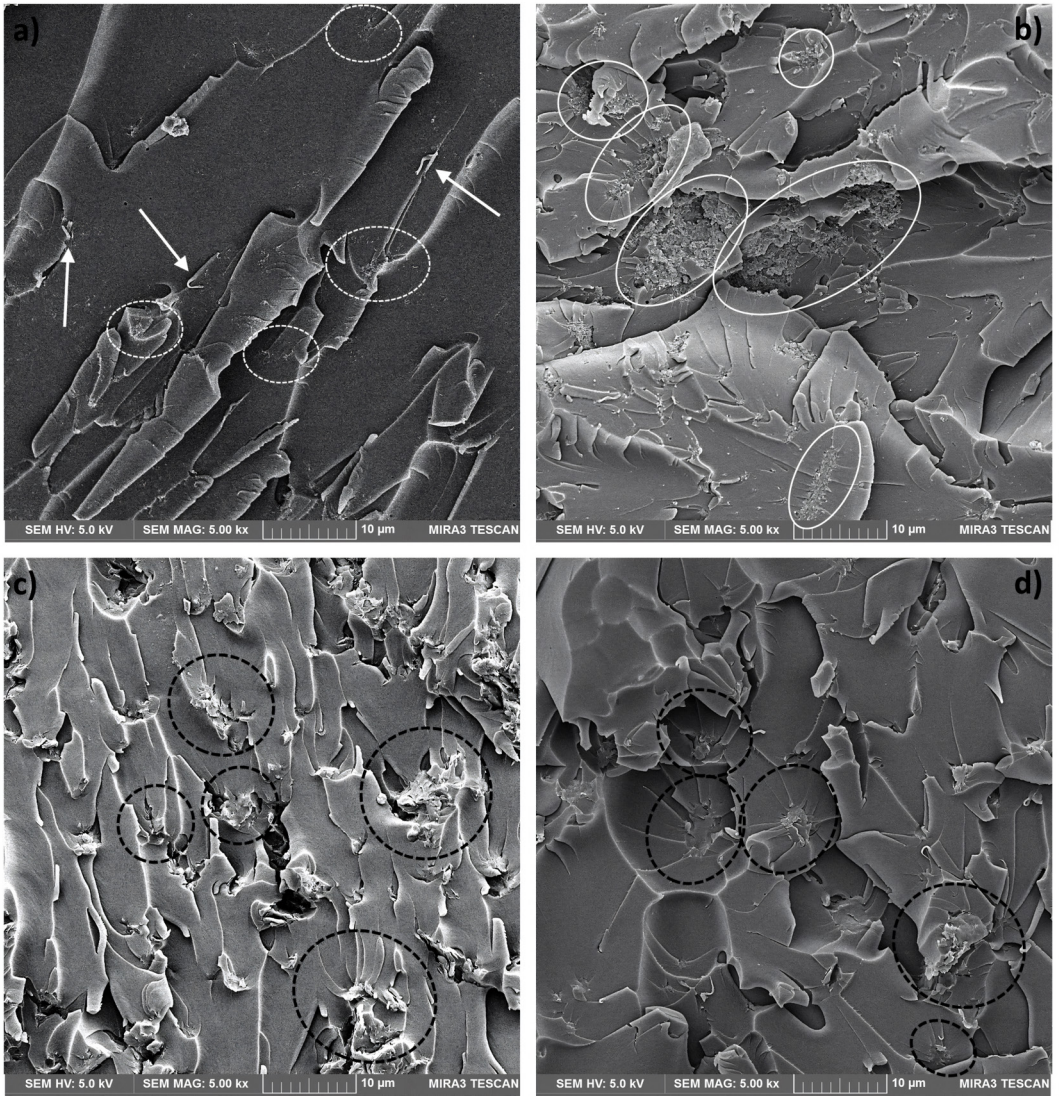

Figure 2. FEG-SEM of the (a) CNT _1.50, (b) Al_1.50, (c) MMT B_1.50 and (d) MMT A_1.50 samples. Circled regions indicate the presence of nanoparticles on the fracture surface and arrows highlight a fractographic aspect.

of large agglomerates. However, the TEM image for this sample (Figure 3b) suggests that the alumina nanoparticles formed an interconnected network extending for dimensions much larger than the nanoparticle diameter itself. This interconnected network could decrease the mobility of the surrounding epoxy resin.

Finally, nanoclay nanocomposites exhibit very similar behavior, independently of the nanoclay type. TEM images (Figures 3c,d) for both show the existence of large tactoids with a discrete exfoliated state on their limits. This behavior is more evident in the case of MMT-Na^+ nanocomposite and can be identified by the misty aspect surrounding the tactoids (recognized by the thin darker lines). Figure 2c and Figure 2d show that these tactoids interact with the crack propagation promoting its deviation, which can be seen by the numerous crack planes. Another piece of evidence are the river lines and scarps emerging from coincident points (highlighted by black circles), in this case, the stress concentrations caused by the tactoids.

3.2. Electrical characterization

All samples were evaluated via DC conductivity measurements using the two-probe method. However, all composites presented electrical conductivity below the reliable detection limit of equipment, thus making the use of these data unfeasible. Therefore, the following discussion is based only on AC conductivity measurements.

Electric permittivity is a complex parameter revealing two components: the real part related to the energy storage in the material and the imaginary counterpart defined as the losses of stored energy. The sum of both contributions is the relative electric permittivity or dielectric constant, which depends on frequency. In other words, permittivity is a dielectric property that measures the displacement of charge carriers in the material when exposed to an electric field. Figure 4a details the permittivity results with the highest concentration of all studied nanoparticles. This figure shows that the dielectric constants decrease with

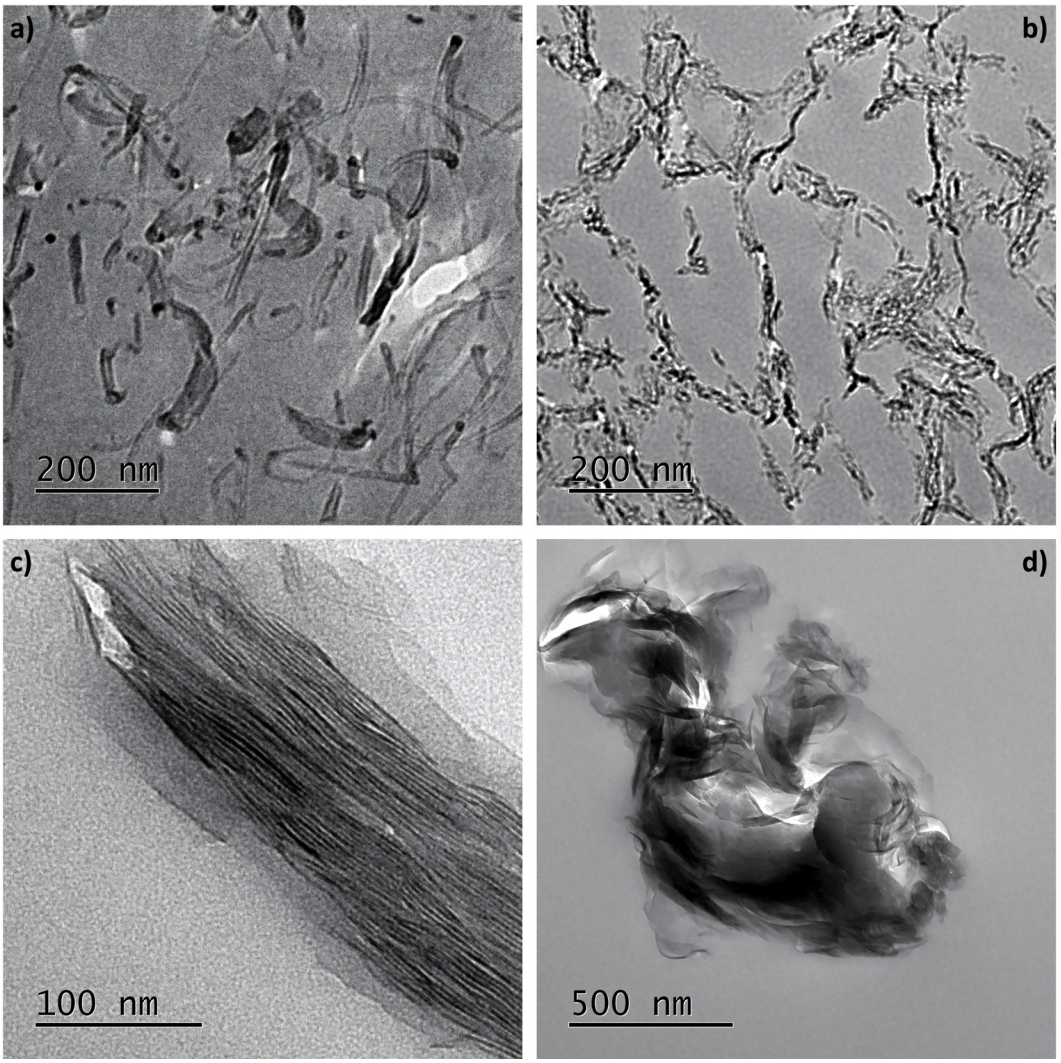

Figure 3. TEM of the (a) CNT _1.50, (b) Al_1.50, (c) MMT B_1.50 and (d) MMT A_1.50 samples.

increasing frequency, with a similar tendency for the curves of MMTs and Al nanofillers, which converge together for higher frequencies. This behavior can be attributed to the low concentration that does not favor the percolated pathways in the composites and limits the polarization effect, which is believed to be the main mechanism of dielectric loss in nanocomposites[33,34]. Similar behavior is observed for the CNT-based nanocomposites, but with higher values, probably due to the nanotubes forming more networks.

Specimens with higher nanoclay amounts (MMT A_1.50 and MMT B_1.50), nanoalumina (Al_1.50) presented an insignificant increase in dielectric properties since the values of relative permittivity are in the same order of magnitude than that epoxy resin (ε_r = 3.00 – 4.54, at 1 kHz). The addition of CNTs (CNT_0.15, CNT_0.50, and CNT_1.50), on the other hand, suggests an increased number of polarizable dipoles, resulting in a positive outcome for the relative permittivity (ε_r = 62.33 – 224.95, at 1 kHz). The dispersion of CNT inside the matrix provides polarization centers due to the accumulation of charges at the interfaces between the resin and the nanoparticles, resulting in increased dielectric constant[33].

Regarding AC electrical conductivity, as shown in Figure 4b, except for composites with CNTs, it is noted that the behavior of all samples is typical of electrical insulator materials, with conductivity ranging from 1.17 to 2.67 x 10^{-9} at 1 kHz, and increasing proportionally with the frequency, from 10 Hz. The increase in conductivity observed from 10 Hz onwards, as the frequency increases, can be attributed to the electron hopping that dominates AC electrical conductivity over DC conductivity (static electrical conductivity)[33,34]. On the other hand, CNT composites present constant conductivity up to a critical frequency[35]. Below the crucial frequency (~10^4 Hz), electron transport occurs by the transfer of charge carriers between CNTs with long-distance transport prevalence. Thus, the AC conductivity of the material assumes the value of DC conductivity due to the formation of a percolative network. Above the critic frequency, higher frequencies lead to electron transport within an unique CNT with no more contact resistance between the particles, reducing the electrical resistance[36].

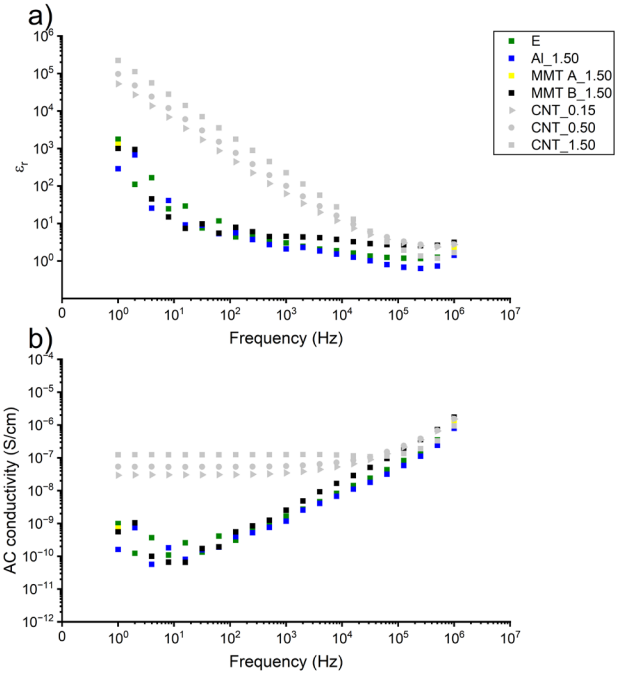

Figure 4. Relative electrical permittivity (a) and alternating electrical conductivity (b) of the nanocomposites prepared with the highest concentrations of nanofillers.

Besides, the conductivity increases with increasing the CNT concentration (3.47 – 12.5 x 10^{-8}, at 1 kHz) as well as the frequency of inversion (~10^4 - ~10^5 Hz). Therefore, a broad region of the conductivity curve is independent of frequency, evidencing the densification of the conductive network and the reduction of the distance between the CNTs inside the matrix, as discussed in the literature[37,38]. The results obtained from σ_{AC} and ε_r of the samples with higher loadings are presented in Table 2.

The semiconductive compositions of CNTs with different concentrations (CNT_0.15, CNT_0.50, and CNT_1.50) were evaluated by the impedance complex plane plot, that is, negative imaginary impedance (Z") *versus* real impedance (Z') (Figure 5) (Nyquist plots). All nanocomposites shown in Figure 5 exhibit a characteristic impedance response with a semicircle shape indicating the presence of polarization with a single relaxation time. The deviation from the ideal semicircular may indicate the presence of heterogeneities in the samples, like bubbles or agglomerates[39]. In the context of the studied composite materials, the appearance of a semicircle on the Nyquist plot can indicate impedance associated with interfaces between different phases, which combines resistive (positive Z') and capacitive effects (negative Z"). That is, in addition to electrical losses due to the Joule effect usually observed in a DC system, the samples can also be compounded by effects that oppose phase changes in an AC circuit (capacitance and inductance). The studied CNTs based composites showed primarily a capacitive behavior with semicircles, whose diameters decrease with increasing reinforcement concentration. The smaller radius of the semicircle represents higher electrical conductivity while the center of the semicircle represents the distance between nanofiller particles[40].

3.3. Electromagnetic characterization

Figure 6 presents the influence of the incorporation of different reinforcements on the power balance of epoxy composites. It is noted that emitting electromagnetic signals in composites of nanoalumina and nanoclays at the highest concentration (1.5% vol.) results in the transmission of most of the energy, with T ranging from 0.63-0.65 mW, at 10 GHz. The microwave transparency of nanoalumina, as observed for epoxy resin (T = 0.67 mW, at 10 GHz), is expected due to the highly insulating behavior of these nanoparticles. However, Rani et al. demonstrate that the addition of 5 wt% of MMT led to a decrease in the energy transmitted through an insulating matrix of poly(vinyl chloride) (PVC)[25]. The observed behavior was attributed to the high aspect ratio of the nanoparticles used and the good dispersion of MMT within the polymeric matrix. The literature also mentions an increase in attenuated energy by the addition of nanoclays due to the increase in system moisture. In this case, water molecules present in the structure of nanoclay act as dipoles interacting with the EM wave[41]. The preponderant transparency of composites formulated with ceramic particles is promising for applications that require this property.

The incorporation of CNTs resulted in a synergistic effect of reflection (R = 0.35 - 0.54 mW, at 10 GHz) and absorption (A = 0.09 - 0.12 mW, at 10 GHz), leading to the highest values of attenuation of electromagnetic energy observed (T = 0.34 mW, at 10 GHz) among the most concentrated samples.

Figure 7 and Table 3 illustrate the positive trend in epoxy shielding properties with the progressive increase in the volume of carbon loads, which has more significant results compared to nanoclay and nanoalumina fillers. Above the intermediate concentration of 0.5% vol. of CNTs, there is a

Table 2. AC electrical conductivity and relative electrical permittivity of the nanocomposites prepared with the highest concentrations of fillers at 1 kHz.

Samples	$\sigma_{AC\ (S/cm)}$	ε_r
E	1.68 x 10^{-9}	3.02
MMT A _1.50	2.67 x 10^{-9}	4.80
MMT B _1.50	2.53 x 10^{-9}	4.54
Al_1.50	1.17 x 10^{-9}	2.10
CNT_0.15	3.47 x 10^{-8}	62.33
CNT _0.50	5.59 x 10^{-8}	100.46
CNT _1.50	1.25 x 10^{-7}	224.95

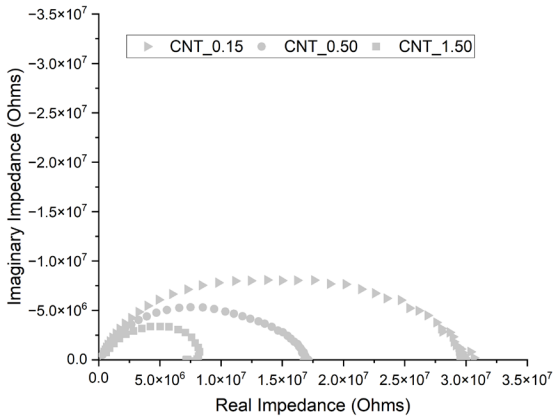

Figure 5. Impedance spectroscopy complex-plane plot (or Nyquist Plot) for the CNTs based nanocomposites.

transition in the electromagnetic behavior of the composites, with the material blocking more than half of the incident energy, being predominantly reflector in the most concentrated sample (1.5% vol: R = 0.54 mW, at 10 GHz). In addition, absorption increases progressively, which is in agreement with the electrical percolation of all CNT composites, leading to higher losses by resistive effect.

Microwave absorption depends heavily on the electrical permittivity and magnetic permeability of the material. The real components of both parameters are defined as the energy stored, whereas the imaginary counterparts are related to the energy losses. The discrepancy between the values of μ and ε tends to intensify reflections, while higher values of ε" and μ" increase the attenuation of the electromagnetic wave[42]. Therefore, the addition of conductive particles, such as CNT, improves the shielding properties by increasing electrical conductivity but compromises the impedance matching. Non-magnetic materials, such as the samples under study, have low μ_r resulting in the reflection of the electromagnetic wave due to the mismatch between permittivity and permeability.

Therefore, it is evident that the increase in reflected energy relies on the improvement of the real permittivity of CNT (ε' = 3.32 – 5.33, at 10 GHz) compared to epoxy resin (ε' = 2.85 and ε" = 0.11, at 10 GHz). The improved imaginary values (ε" = 0.20 - 0.70, at 10 GHz) provide higher loss tangent (tan δ = ε"/ε'), which indicates the ability to convert stored energy into heat. The relative permittivity/loss tangent and the power balance of CNT composites are shown in Figure 8 and Table 3, respectively.

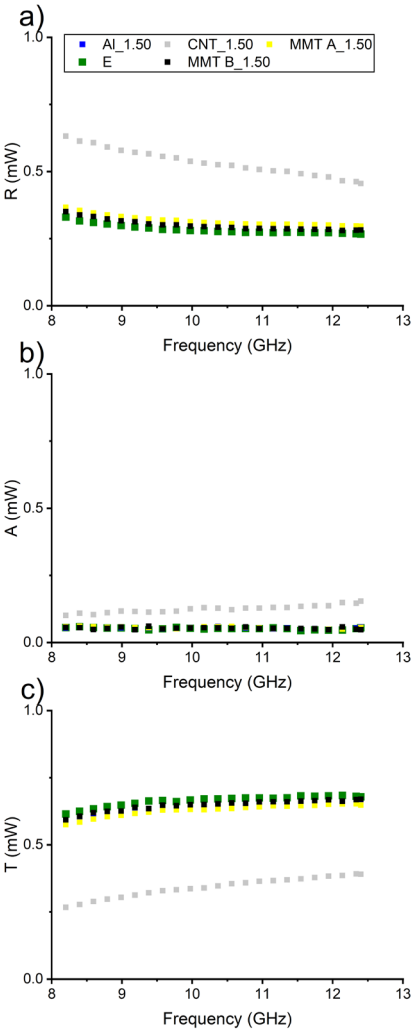

Figure 6. Values of (a) R, (b) A and (c) T of nanocomposites prepared with the highest concentrations of nanofillers.

Different authors establish that the minimum electromagnetic shielding efficiency required for commercial applications is around 20 dB (decibel), which means the incident wave should be attenuated by 99%[23,43-45]. The SE_T of CNT composites, at 10 GHz, showed values of 2.55 dB, 3.51 dB, and 4.71 dB for the CNT_0.15, CNT_0.50, and CNT_1.50 samples, respectively (Figure 9 and Table 4), that is, below the commercial requirements.

Despite the unenthusiastic results, previous works show suitable shielding results with higher nanofiller loadings in polymeric matrices and by applying novel strategies, such as ternary composites, sandwich structures, and reticulated (foam) structures[46-49]. Nevertheless, it is noticeable that CNTs nanoparticles can improve the shielding properties of polymer composites at low concentrations. Reflection loss increases with the incorporation of conductive nanoparticles, as can be seen in the CNT samples with SE_R ranging from 1.89 - 3.38 dB (10 GHz). Absorption loss requires moderate electrical conductivity, which is achieved due to the formation of a conductive network as seen in CNT samples (SE_A = 0.65 – 1.33 dB, at 10 GHz).

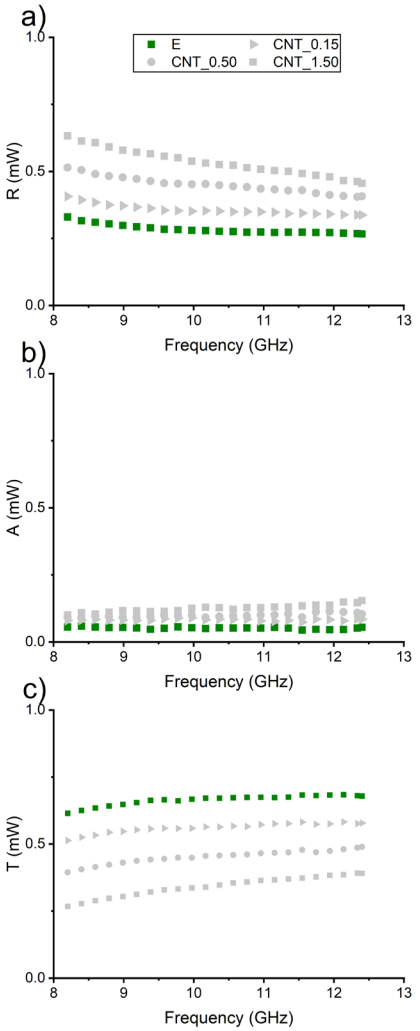

Figure 7. Values of (a) R, (b) A and (c) T of nanocomposites prepared with different concentrations of CNTs.

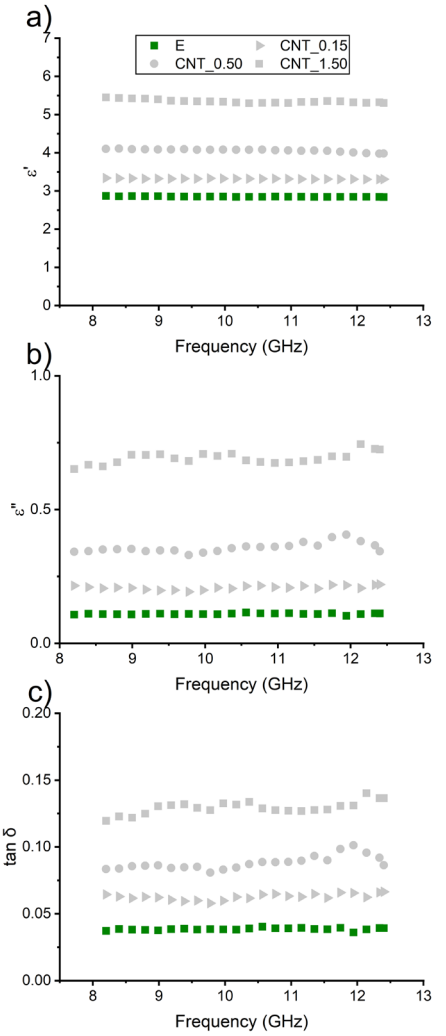

Figure 8. Values of ε' (a), ε" (b) and tan δ (c) of nanocomposites with CNTs.

Table 3. Power balance and relative complex permittivity and its components at 10 GHz.

Sample	R	T	A	ε'	ε"	ε"/ ε'	ε_r
E	0.28	0.67	0.05	2.85	0.11	0.04	2.85
MMT A _1.50	0.31	0.63	0.05	3.04	0.12	0.04	3.04
MMT B _1.50	0.30	0.65	0.05	2.94	0.11	0.04	2.95
Al_1.50	0.31	0.64	0.05	3.00	0.12	0.04	3.00
CNT_0.15	0.35	0.56	0.09	3.32	0.20	0.06	3.33
CNT _0.50	0.45	0.45	0.10	4.08	0.35	0.08	4.09
CNT _1.50	0.54	0.34	0.12	5.33	0.70	0.13	5.37

Table 4. SE_A, SE_R and SE_T of CNTs nanocomposites, at 10 GHz, and reflection loss results.

Sample	SE_A (dB)	SE_R (dB)	SE_T (dB)	SE_T (%)	RL (dB)	RL (%)
E	0.31	1.43	1.75	33.2	-0.94 at 12.4 GHz	19.5 at 12.4 GHz
CNT_0.15	0.65	1.89	2.55	44.4	-1.81 at 12.4 GHz	34.1 at 12.4 GHz
CNT _0.50	0.90	2.61	3.51	55.4	-4.28 at 12.1 GHz	62.7 at 12.1 GHz
CNT _1.50	1.33	3.38	4.71	66.2	-6.61 at 10.8 GHz	78.2 at 10.8 GHz

Another point of interest is the decrease of reflection loss with increasing frequency, whereas the absorption remains practically the same (Figure 9). The frequency-independent shielding properties of absorbing materials are another advantage, resulting in virtually constant attenuation over a wide range of frequencies since the mechanisms of radiation conversion into heat show no variation with frequency. Thus, a more detailed study of absorbing materials is urgent for efficient electromagnetic shielding materials.

One of the requirements for absorption-dominant structures is air/material impedance matching, which leads to a minimum of reflection loss (RL) on the front face of the material[50]. In addition, maximum absorption is achieved by balancing the dielectric and magnetic properties of the shielding. However, dielectric absorbers possess high electrical permittivity and discrete permeability ($\mu_r <<< \varepsilon_r$), leading to reflection losses and compromising the electromagnetic wave transmission inside the material. The analysis of Table 4 shows, in general, that the samples studied present low SE_R, indicating a satisfactory impedance matching, that is, the reflection on the first surface of the samples is low, so the propagation of the wave through the material is favored. However, the RL values of the epoxy resin and CNT_0.15 samples show insignificant attenuation values (-0.94 dB and -1.81 dB, respectively). The correlation of SE_R and RL of these two samples indicates that these materials behaved as transparent materials. In these cases, the incident wave that propagated through the material was reflected upon reaching the metal plate at the back of the sample in the sample-holder, resulting in negligible attenuation of the wave. The more concentrated samples (CNT_0.50 and CNT_1.50) present more significant SE_R (0.90 – 1.33 dB) and SE_A (2.61 – 3.38 dB) values. In these two cases, the reflection on the surface of the samples is not yet very significant. Even so, the SE_A is higher, favoring greater wave energy losses into the material, contributing to increase the RL values (-4.28 dB and -6.61 dB). Probably these dielectric losses are caused by polarization loss and ohmic loss[51].

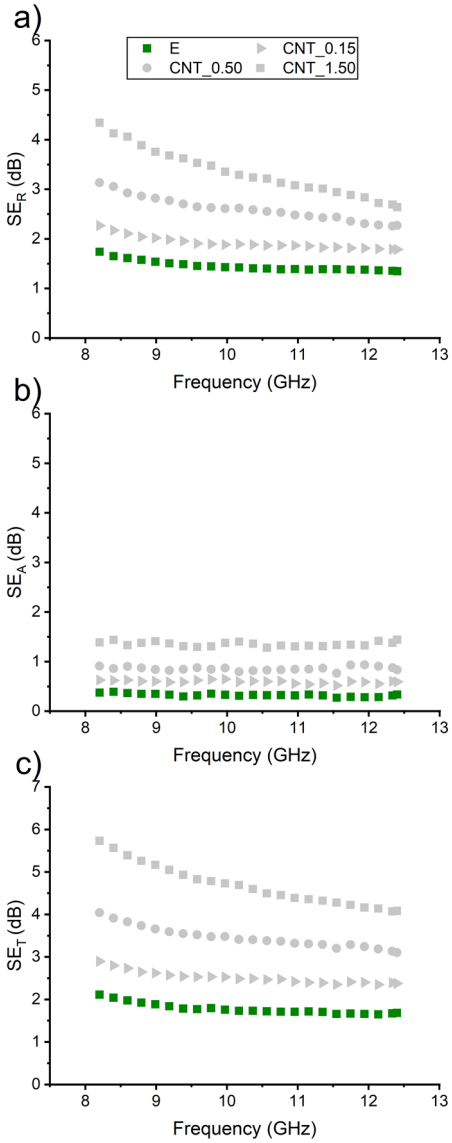

Figure 9. Electromagnetic shielding curves of losses by reflection (a), absorption (b) and total attenuation (c) of nanocomposites with CNTs.

The reflection loss behavior of CNTs based composites in the X-band is shown in Figure 10. The most concentrated CNTs (1.5%.vol) sample presents a minimum reflection loss of -6.61 dB (78.5% of attenuation), at 10.8 GHz. The dip appearance of reflection loss seen in the curves can be related to the match between the physical thickness of the absorber with the one-quarter wavelength condition[52-54]. When the thickness of the shield equals the odd-numbered multiple of the quarter of the incident wavelength, the phase difference between the incident wave and the reflected wave becomes 180° at the air/shield interface. This results in the cancelation between the reflected wave and the incident wave at the air/shield interface, revealing a resonant peak[8,55].

Efficient absorbing materials are associated with reflection loss values below -10 dB and adequate bandwidth[56]. Table 5 shows the results of this study and the shielding properties of epoxy composites obtained in the literature. As can be seen, high microwave absorption can be achieved with higher

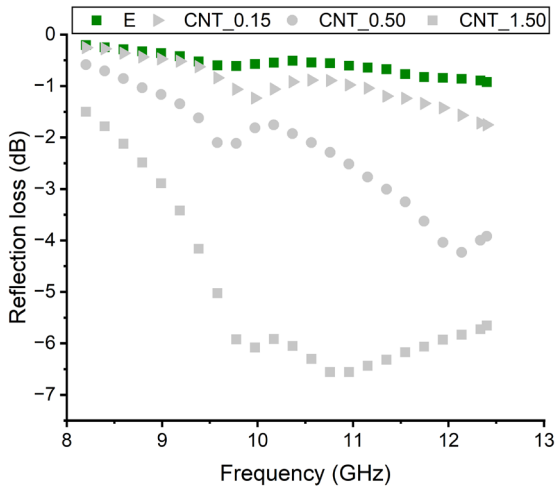

Figure 10. Reflection loss in the X-band of the nanocomposites with CNTs.

Table 5. Review of previously published articles in the literature.

Material	Thickness (mm)	EMI SE / RL (dB)	Band	Reference
		EMI SE		
Epoxy/CNTs (15 wt%)	2	25	8.2-12.4 GHz	[57]
Epoxy/CNTs (2.5 wt%)	2	8	8.2-12.4 GHz	[58]
Epoxy/CNTs (1.5 vol%)	3	4.5	8.2-12.4 GHz	This work
		Reflection loss (RL)		
Epoxy/CNTs (20.7 wt%)	1.75	−19	8.2-12.4 GHz	[59]
Epoxy/CNTs (2.0 wt%)	3	−10.5	8.2-12.4 GHz	[60]
Epoxy/CNTs (1.5 vol%)	3	-6.6	8.2-12.4 GHz	This work

nanofiller loadings due to more significant dielectric losses without altering the impedance matching. Moreover, similar concentrations of CNTs analyzed in this study present no reflection loss equal to or higher than those found in Table 5. The difference can be associated with the different particle orientations and the properties of the CNTs used (aspect ratio, electrical conductivity, defects, length, among others), resulting in mild microwave absorption in the present study.

4. Conclusions

CNTs, nanoclays, and nanolumina reinforced epoxy composites (0.15, 0.50, and 1.50% vol.) were characterized by seeking electromagnetic shielding application. The as-prepared composites do not meet the requirements for commercial application (EMI SE > 20 dB) due to their low shielding performance. Despite the need for optimization, CNTs demonstrate a low electrical percolation threshold (0.15%) and remarkable potential as a reinforcing material for electromagnetic interference (EMI) shielding compared to other studied alternatives, improving both reflection and absorption losses. This is due to its high aspect ratio and electrical conductivity, which contributes to the formation of a conductive network of nanoparticles. It is expected that higher loadings of CNTs or more intricate morphology approaches such as sandwich structures, foams, and hybrid composites could lead to efficient EMI shielding composites based on CNTs.

Nanoclays and nanoalumina revealed no improvement in the conductivity and poor shielding/absorption properties. However, this result is suitable for applications that require preponderant microwave transparency of the final product.

Electromagnetic characterization revealed the predominantly reflective behavior of composites. The increase in electromagnetic shielding was proportional to the nanofiller concentration, where the most concentrated CNT sample (1.50% vol) showed the most promising results (SE_T = 4.7 dB). CNT showed potential for the conceptualization of absorbing and shielding materials. Reflectivity measurements confirm this trend revealing attenuation values of -6.6 dB (78.5% of attenuation) at 10.8 GHz.

5. Acknowledgments

The authors would like to thank the Brazilian Funding Institutions CNPq (Conselho Nacional de Desenvolvimento Científico e Tecnológico. Project: 306836/2023-8) and FAPESP (Fundação de Amparo à Pesquisa do Estado de São Paulo, Project: 2017/04740-0, 2019/01623-8) for financial support, the Instituto Nacional de Pesquisas Espaciais (INPE, Brazil) for electromagnetic analyses, the Laboratório de Cerâmica Avançada of the Instituto de Ciência e Tecnologia/UNIFESP for electrical measurements, and also MSc. Erick G. R. dos Anjos for his support in the discussion of the Nyquist diagrams.

6. References

1. Abbasi H, Antunes M, Velasco JI. Recent advances in carbon-based polymer nanocomposites for electromagnetic interference shielding. Prog Mater Sci. 2019;103:319-73. http://doi.org/10.1016/j.pmatsci.2019.02.003.
2. Wu N, Hu Q, Wei R, Mai X, Naik N, Pan D, et al. Review on the electromagnetic interference shielding properties of carbon based materials and their novel composites: recent progress, challenges and prospects. Carbon. 2021;176:88-105. http://doi.org/10.1016/j.carbon.2021.01.124.
3. Kumar R, Sahoo S, Joanni E, Singh RK, Tan WK, Kar KK, et al. Recent progress on carbon-based composite materials for microwave electromagnetic interference shielding. Carbon. 2021;177:304-31. http://doi.org/10.1016/j.carbon.2021.02.091.
4. Jiang D, Murugadoss V, Wang Y, Lin J, Ding T, Wang Z, et al. Electromagnetic interference shielding polymers and nanocomposites - a review. Polym Rev (Phila Pa). 2019;59(2):280-337. http://doi.org/10.1080/15583724.2018.1546737.
5. Hu Y, Tang P, Li L, Yang J, Jian X, Bin Y. High absorption shielding material of poly(phthalazinone etherketone)/multiwall carbon nanotube composite films with sandwich configurations. RSC Advances. 2019;9(33):18758-66. http://doi.org/10.1039/C9RA02959A.
6. Singh AK, Shishkin A, Koppel T, Gupta N. A review of porous lightweight composite materials for electromagnetic interference shielding. Compos, Part B Eng. 2018;149:188-97. http://doi.org/10.1016/j.compositesb.2018.05.027.
7. Rouhi M, Hajizadeh Z, Taheri-Ledari R, Maleki A, Babamoradi M. A review of mechanistic principles of microwave absorption by pure and composite nanomaterials. Mater Sci Eng B. 2022;286:116021. http://doi.org/10.1016/j.mseb.2022.116021.
8. Ruiz-Perez F, López-Estrada SM, Tolentino-Hernández RV, Caballero-Briones F. Carbon-based radar absorbing materials: a critical review. Journal of Science: Advanced Materials and Devices. 2022;7(3):100454. http://doi.org/10.1016/j.jsamd.2022.100454.
9. Hema S, Sambhudevan S. Ferrite-based polymer nanocomposites as shielding materials: a review. Chem Pap. 2021;75(8):3697-710. http://doi.org/10.1007/s11696-021-01664-1.
10. Bhaskaran K, Bheema RK, Etika KC. The influence of Fe3O4@GNP hybrids on enhancing the EMI shielding effectiveness of epoxy composites in the X-band. Synth Met. 2020;265:116374. http://doi.org/10.1016/j.synthmet.2020.116374.
11. Pu L, Li S, Zhang Y, Zhu H, Fan W, Ma P, et al. Polyimide-based graphene composite foams with hierarchical impedance

gradient for efficient electromagnetic absorption. J Mater Chem C Mater Opt Electron Devices. 2021;9(6):2086-94. http://doi.org/10.1039/D0TC04951D.
12. Network N, Frequency L, Vovchenko L, Matzui L, Oliynyk V, Milovanov Y. Polyethylene composites with segregated carbon high electromagnetic interference. Materials (Basel). 2020;13:1-14.
13. Ghaffoori AJ, Abdul-Adheem WR. A review of carbon nanotubes electrical properties for future nanotechnology applications. Al-Rafidain J Sci. 2019:45(2):207-22. https://doi.org/10.55562/jrucs.v45i2.123.
14. Alemour B, Yaacob MH, Lim HN, Hassan MR. Review of electrical properties of graphene conductive composites. International Journal of Nanoelectronics and Materials. 2018;11:371-98.
15. Zhu S, Xing C, Wu F, Zuo X, Zhang Y, Yu C, et al. Cake-like flexible carbon nanotubes/graphene composite prepared via a facile method for high-performance electromagnetic interference shielding. Carbon. 2019;145:259-65. http://doi.org/10.1016/j.carbon.2019.01.030.
16. Zhao B, Wang S, Zhao C, Li R, Hamidinejad SM, Kazemi Y, et al. Synergism between carbon materials and Ni chains in flexible poly(vinylidene fluoride) composite films with high heat dissipation to improve electromagnetic shielding properties. Carbon. 2018;127:469-78. http://doi.org/10.1016/j.carbon.2017.11.032.
17. Wei L, Zhang W, Ma J, Bai S-L, Ren Y, Liu C, et al. π-π stacking interface design for improving the strength and electromagnetic interference shielding of ultrathin and flexible water-borne polymer/sulfonated graphene composites. Carbon. 2019;149:679-92. http://doi.org/10.1016/j.carbon.2019.04.058.
18. Liu Y-F, Feng L-M, Chen Y-F, Shi Y-D, Chen X-D, Wang M. Segregated polypropylene/cross-linked poly(ethylene-co-1-octene)/multi-walled carbon nanotube nanocomposites with low percolation threshold and dominated negative temperature coefficient effect: towards electromagnetic interference shielding and thermistors. Compos Sci Technol. 2018;159:152-61. http://doi.org/10.1016/j.compscitech.2018.02.041.
19. Wu H-Y, Jia L-C, Yan D-X, Gao J, Zhang X-P, Ren P-G, et al. Simultaneously improved electromagnetic interference shielding and mechanical performance of segregated carbon nanotube/polypropylene composite via solid phase molding. Compos Sci Technol. 2018;156:87-94. http://doi.org/10.1016/j.compscitech.2017.12.027.
20. Yu W-C, Zhang G-Q, Liu Y-H, Xu L, Yan D-X, Huang H-D, et al. Selective electromagnetic interference shielding performance and superior mechanical strength of conductive polymer composites with oriented segregated conductive networks. Chem Eng J. 2019;373:556-64. http://doi.org/10.1016/j.cej.2019.05.074.
21. dos Reis FC, Gomes NAS, Baldan MR, Ribeiro B, Rezende MC. The influence of carbonyl iron and magnetite ferrite on the electromagnetic behavior of nanostructured composites based on epoxy resin/buckypapers. J Magn Magn Mater. 2022;563:170007. http://doi.org/10.1016/j.jmmm.2022.170007.
22. dos Anjos EGR, Marini J, Gomes NAS, Rezende MC, Passador FR. Synergistic effect of adding graphene nanoplates and carbon nanotubes in polycarbonate/acrylonitrile-styrene-butadiene copolymer blend. J Appl Polym Sci. 2022;139(37):e52873. http://doi.org/10.1002/app.52873.
23. dos Anjos EGR, Moura NK, Antonelli E, Baldan MR, Gomes NAS, Braga NF, et al. Role of adding carbon nanotubes in the electric and electromagnetic shielding behaviors of three different types of graphene in hybrid nanocomposites. J Thermoplast Compos. 2023;36(8):3209-35. http://doi.org/10.1177/08927057221124483.
24. dos Reis FC, Rezende MC, Ribeiro B. The influence of the transparent layer thickness on the absorption capacity of epoxy/carbon nanotube buckypaper at X-band. J Appl Polym Sci. 2021;138(47):1-11. http://doi.org/10.1002/app.51407.
25. Rani P, Ahamed MB, Deshmukh K. Significantly enhanced electromagnetic interference shielding effectiveness of montmorillonite nanoclay and copper oxide nanoparticles based polyvinylchloride nanocomposites. Polym Test. 2020;91:106744. http://doi.org/10.1016/j.polymertesting.2020.106744.
26. Joseph J, Koyadan AK, Sidpara AM, Paul J. Microwave shielding characteristics of thermoplastic/graphene composites with montmorillonite (bentonite) clay addition for improved thermal stability. Polymer-Plastics Technology and Materials. 2022;61(3):283-95. http://doi.org/10.1080/25740881.2021.1982968.
27. Osman A, Elhakeem A, Kaytbay S, Ahmed A. Thermal, electrical and mechanical properties of graphene/nano-alumina/epoxy composites. Mater Chem Phys. 2021;257:123809. http://doi.org/10.1016/j.matchemphys.2020.123809.
28. Opelt CV, Coelho LAF. Reinforcement and toughening mechanisms in polymer nanocomposites - Reinforcement effectiveness and nanoclay nanocomposites. Mater Chem Phys. 2016;169:179-85. http://doi.org/10.1016/j.matchemphys.2015.11.047.
29. Opelt CV, Becker D, Lepienski CM, Coelho LAF. Reinforcement and toughening mechanisms in polymer nanocomposites - Carbon nanotubes and aluminum oxide. Compos, Part B Eng. 2015;75:119-26. http://doi.org/10.1016/j.compositesb.2015.01.019.
30. Opelt CV, Coelho LAF. On the pseudo-ductility of nanostructured epoxy resins. Polym Test. 2019;78:105961. http://doi.org/10.1016/j.polymertesting.2019.105961.
31. Yun T, Kim H, Iqbal A, Cho YS, Lee GS, Kim MK, et al. Electromagnetic shielding of monolayer MXene assemblies. Adv Mater. 2020;32(9):1-9. http://doi.org/10.1002/adma.201906769.
32. Greenhalgh E. Failure analysis and fractography of polymer composites. Cambridge: Woodhead; 2009.
33. Hu H, Zheng Y, Ren K, Wang J, Zhang Y, Zhang X, et al. Position selective dielectric polarization enhancement in CNT based heterostructures for highly efficient microwave absorption. Nanoscale. 2021;13(4):2324-32. http://doi.org/10.1039/D0NR08245G.
34. Ravindran AR, Feng C, Huang S, Wang Y, Zhao Z, Yang J. Effects of graphene nanoplatelet size and surface area on the AC electrical conductivity and dielectric constant of epoxy nanocomposites. Polymers (Basel). 2018;10(5):477. http://doi.org/10.3390/polym10050477.
35. Al-Saleh MH, Al-Anid HK, Husain YA, El-Ghanem HM, Jawad SA. Impedance characteristics and conductivity of CNT/ABS nanocomposites. J Phys D Appl Phys. 2013;46(38):385305. http://doi.org/10.1088/0022-3727/46/38/385305.
36. Barrau S, Demont P, Peigney A, Laurent C, Lacabanne C. Dc and ac conductivity of carbon nanotubes-polyepoxy composites. Macromolecules. 2003;36(14):5187-94. http://doi.org/10.1021/ma021263b.
37. Vavouliotis A, Fiamegou E, Karapappas P, Psarras GC, Kostopoulos V. DC and AC conductivity in epoxy resin/multiwall carbon nanotubes percolative system. Polym Compos. 2010;31(11):1874-80. http://doi.org/10.1002/pc.20981.
38. Zhao B, Wang R, Li Y, Ren Y, Li X, Guo X, et al. Dependence of electromagnetic interference shielding ability of conductive polymer composite foams with hydrophobic properties on cellular structure. J Mater Chem C Mater Opt Electron Devices. 2020;8(22):7401-10. http://doi.org/10.1039/D0TC00987C.
39. dos Anjos EGR, Brazil TR, de Melo Morgado GF, Montagna LS, Braga NF, Antonelli E, et al. Influence of MWCNT aspect ratio on the rheological, electrical, electromagnetic shielding, and mechanical properties of polycarbonate melt mixed nanocomposites. J Polym Res. 2023;30(2):89. http://doi.org/10.1007/s10965-023-03453-8.
40. dos Anjos EGR, Brazil TR, de Melo Morgado GF, Antonelli ENC, Medeiros NCFL, Santos AP, et al. de F.L. Medeiros, A.P. Santos, T. Indrusiak, M.R. Baldan, M.C. Rezende, L.A. Pessan, F.R. Passador, Graphene related materials as effective

additives for electrical and electromagnetic performance of epoxy nanocomposites. FlatChem. 2023;41:100542. http://doi.org/10.1016/j.flatc.2023.100542.
41. Nigil MR, Ramanujam BTS, Thiruvengadathan R. Nanoclay-based Polymer Nanocomposites for Electromagnetic Interference Shielding. Advanced Applications of Micro and Nano Clay II. 2022;129:53-78. http://doi.org/10.21741/9781644902035-3.
42. Green M, Chen X. Recent progress of nanomaterials for microwave absorption. Journal of Materiomics. 2019;5(4):503-41. http://doi.org/10.1016/j.jmat.2019.07.003.
43. Tang W, Lu L, Xing D, Fang H, Liu Q, Teh KS. A carbon-fabric/polycarbonate sandwiched film with high tensile and EMI shielding comprehensive properties: an experimental study. Compos, Part B Eng. 2018;152:8-16. http://doi.org/10.1016/j.compositesb.2018.06.026.
44. Vargas PC, Merlini C, da Silva Ramôa SDA, Arenhart R, de Oliveira Barra GM, Soares BG. Conductive composites based on polyurethane and nanostructured conductive filler of montmorillonite/polypyrrole for electromagnetic shielding applications. Mater Res. 2018;21(5):e20180014. http://doi.org/10.1590/1980-5373-mr-2018-0014.
45. Kuester S, Demarquette NR, Ferreira JC Jr, Soares BG, Barra GMO. Hybrid nanocomposites of thermoplastic elastomer and carbon nanoadditives for electromagnetic shielding. Eur Polym J. 2017;88:328-39. http://doi.org/10.1016/j.eurpolymj.2017.01.023.
46. Liang C, Gu Z, Zhang Y, Ma Z, Qiu H, Gu J. Structural Design Strategies of Polymer Matrix Composites for Electromagnetic Interference Shielding: A Review. Nano-Micro Lett. 2021;13(1):1-29. http://doi.org/10.1007/s40820-021-00707-2.
47. Wang H, Li S, Liu M, Li J, Zhou X. Review on Shielding Mechanism and Structural Design of Electromagnetic Interference Shielding Composites. Macromol Mater Eng. 2021;306(6):1-13. http://doi.org/10.1002/mame.202100032.
48. Zhong L, Yu R, Hong X. Review of carbon-based electromagnetic shielding materials: film, composite, foam, textile. Text Res J. 2021;91(9-10):1167-83. http://doi.org/10.1177/0040517520968282.
49. Zhao B, Zeng S, Li X, Guo X, Bai Z, Fan B, et al. Flexible PVDF/carbon materials/Ni composite films maintaining strong electromagnetic wave shielding under cyclic microwave irradiation. J Mater Chem C Mater Opt Electron Devices. 2020;8(2):500-9. http://doi.org/10.1039/C9TC05462F.
50. Zhao B, Deng J, Zhang R, Liang L, Fan B, Bai Z, et al. Recent advances on the electromagnetic wave absorption properties of Ni based materials. Engineered Science. 2018;3:5-40. http://doi.org/10.30919/es8d735.
51. Zhao B, Li Y, Ji H, Bai P, Wang S, Fan B, et al. Lightweight graphene aerogels by decoration of 1D CoNi chains and CNTs to achieve ultra-wide microwave absorption. Carbon. 2021;176:411-20. http://doi.org/10.1016/j.carbon.2021.01.136.
52. Soares BG, Barra GMO, Indrusiak T. Conducting polymeric composites based on intrinsically conducting polymers as electromagnetic interference shielding/microwave absorbing materials: a review. Journal of Composites Science. 2021;5(7):173. http://doi.org/10.3390/jcs5070173.
53. Du C, Zhou D, Guo HH, Pang YQ, Shi HY, Liu WF, et al. An ultra-broadband terahertz metamaterial coherent absorber using multilayer electric ring resonator structures based on anti-reflection coating. Nanoscale. 2020;12(17):9769-75. http://doi.org/10.1039/C9NR10668E.
54. Zhan R, Zhang J, Gao Q, Jia Q, Zhang Z, Zhang G, et al. Microwave absorption performance of single-layer and multi-layer structures prepared by cnts/fe3o4 nonwoven materials. Crystals (Basel). 2021;11(8):1000. http://doi.org/10.3390/cryst11081000.
55. Ribeiro B, Corredor JAR, de Paula Santos LF, Gomes NAS, Rezende MC. Electrical conductivity and electromagnetic shielding performance of glass fiber-reinforced epoxy composites with multiwalled carbon nanotube buckypaper interlayer. J Mater Sci Mater Electron. 2021;32(2):1962-76. http://doi.org/10.1007/s10854-020-04964-6.
56. de Medeiros LI, de Faria Lopes Medeiros NC, Lenz e Silva GFB, de Lima RGA, Amaral-Labat G, Boss AFN, et al. Improved microwave absorption performance with sustainable porous carbon/carbon nanotube composites. Mat Res. 2022;25(suppl 2):e20220169. https://doi.org/10.1590/1980-5373-MR-2022-0169.
57. Huang Y, Li N, Ma Y, Du F, Li F, He X, et al. The influence of single-walled carbon nanotube structure on the electromagnetic interference shielding efficiency of its epoxy composites. Carbon. 2007;45(8):1614-21. http://doi.org/10.1016/j.carbon.2007.04.016.
58. Khodadadi Yazdi M, Noorbakhsh B, Nazari B, Ranjbar Z. Preparation and EMI shielding performance of epoxy/non-metallic conductive fillers nano-composites. Prog Org Coat. 2020;145:105674. http://doi.org/10.1016/j.porgcoat.2020.105674.
59. Singh BP, Bharadwaj P, Choudhary V, Mathur RB. Enhanced microwave shielding and mechanical properties of multiwall carbon nanotubes anchored carbon fiber felt reinforced epoxy multiscale composites. Appl Nanosci. 2014;4(4):421-8. http://doi.org/10.1007/s13204-013-0214-0.
60. Che BD, Nguyen BQ, Nguyen LTT, Nguyen HT, Nguyen VQ, Van Le T, et al. The impact of different multi-walled carbon nanotubes on the X-band microwave absorption of their epoxy nanocomposites. Chem Cent J. 2015;9(1):1-13. http://doi.org/10.1186/s13065-015-0087-2.

Data Availability

The datasets generated during and/or analysed during the current study are available in the Federal university of São Paulo repository, https://repositorio.unifesp.br/handle/11600/66594.